Interdependencies between physical, design and operational parameters for direct use geothermal heat in faulted hydrothermal reservoirs

Daniilidis, Alexandros; Nick, Hamidreza M.; Bruhn, David F.

DOI
10.1016/j.geothermics.2020.101806

Publication date
2020

Document Version
Final published version

Published in
Geothermics

Geothermics 86 (2020) 101806

Contents lists available at ScienceDirect

Geothermics

journal homepage: www.elsevier.com/locate/geothermics

Interdependencies between physical, design and operational parameters for direct use geothermal heat in faulted hydrothermal reservoirs

Alexandros Daniilidis[a,*], Hamidreza M. Nick[b], David F. Bruhn[a,c]

[a] Delft University of Technology, Stewinweg 1, Delft, 2628CN, the Netherlands
[b] Technical University of Denmark, 2800 Kgs, Lyngby, Denmark
[c] GFZ German Research Centre for Geosciences, Telegrafenberg, Potsdam, Germany

ARTICLE INFO

Keywords:
Thermal Hydraulic (TH)
Direct use geothermal
Fault
NPV
Lifetime
Uncertainty
Heat In Place (HIP) recovery
Low-enthalpy

ABSTRACT

Interest in direct use geothermal systems is increasing due to their ability to supply renewable, environmentally friendly heat. Such systems are mostly developed in conduction dominated geological settings where faults are often encountered. Interdependencies between physical, design and operational parameters make it difficult to assess the performance of such systems. Interaction with faults could potentially have adverse effects on system lifetime, generated Net Present Value (NPV) and produced energy. In this work a single doublet system in the enthalpy range of 140 kJ/kg to 350 kJ/kg is analysed using COMSOL Multiphysics. A choice of design (well spacing and placement), physical (layered reservoir, fault flow properties, fault throw) and operational (injection and production flow rates) parameters are considered in a full factorial design that includes 2430 3D reservoir simulations. Results show that fault flow properties characterization is more significant than fault throw structural characterization. For the considered reservoir properties, increasing the flow rate four times results in an NPV increase of a factor seven, despite the shorter system lifetime. A sealing fault renders the system lifetime less sensitive to the doublet positioning. Synthetic model results shown can serve as guidelines to reducing full scale field models. Importance and relevance of these results remains very high for horizontally homogeneous, layered reservoirs. The analysis expands the understanding of interdependencies for direct use geothermal systems and informs on their further development.

1. Introduction

Direct use geothermal systems are mostly developed in conduction dominated fields (Moeck, 2014). These systems are alternatively referred to as Hot Sedimentary Aquifers (HSA), hydrothermal systems, or deep, low enthalpy geothermal systems (Barbier, 2002; Daniilidis et al., 2016a,b; Willems et al., 2017a). A doublet configuration with one producer and one injector well is commonly used (Crooijmans et al., 2016; Slatlem Vik et al., 2018).

Previous studies have focused on examining the performance of such systems controlled by different factors, including fluid properties (Saeid et al., 2014; Watanabe et al., 2010), rock properties (Chandrasiri Ekneligoda and Min, 2014; Mottaghy et al., 2011; Vogt et al., 2013), reservoir heterogeneity (Babaei and Nick, 2019; Liu et al., 2019; Salimzadeh et al., 2019), seasonal fluctuations in discharge and injection temperature (Daniilidis et al., 2017; Saeid et al., 2015), well spacing (Madhur and Anderson, 2012; Willems et al., 2017a) and well positioning and depth (Liang et al., 2018)

For such systems, well spacing has been found to be an important parameter regarding system lifetime but also to the extent that it affects the subdomain area surrounding the doublet (Willems et al., 2017a,b; Willems and Nick, 2019). Moreover, reducing well spacing allows for more doublets to be installed within the same area (Babaei and Nick, 2019; Willems et al., 2017a,b; Willems and Nick, 2019). Additionally, the evaluation of economic output of such a system can vary according to the considered parameters (Daniilidis et al., 2017; Limberger et al., 2018). A geological factor that has been found to influence the produced energy of a geothermal doublet is fault permeability (Blöcher et al., 2010; Daniilidis et al., 2016a,b; Lepillier et al., 2019; Salimzadeh et al., 2018; Salimzadeh and Nick, 2019).

Previous research suggests improved profitability of geothermal projects close to large populations (Knoblauch and Trutnevyte, 2018). Nonetheless, increasing the number of doublets in a given area can lead to interference between neighbouring systems. Negative interference could reduce the recoverable energy with respect to the initial energy potential from a certain geological locality as described in previous

* Corresponding author.
E-mail address: a.daniilidis@tudelft.nl (A. Daniilidis).

https://doi.org/10.1016/j.geothermics.2020.101806
Received 10 September 2019; Received in revised form 25 November 2019; Accepted 18 January 2020

research (Limberger et al., 2018). Fracture flow in discrete fracture systems is shown to impact the thermal performance of reservoirs by effectively controlling the fluid pathway between wells and therefore the system lifetime (Fox et al., 2015). Even if faults are not acting as fluid pathways, pore pressure changes due to injection and production of fluids can still affect the stress distribution of a fault plane (Altmann et al., 2014).

The influence of large faults on the thermal breakthrough and therefore the system lifetime and economic performance of a deep, conduction dominated - geothermal system remains underexplored. In this work we present a coupled, synthetic Thermal-Hydraulic (TH) model using the Finite Element Method (FEM). The model is profiling a sedimentary aquifer, between an impermeable basement and overburden. A parametric study is carried out for a single doublet, producing from the reservoir interval and is laterally bound between two faults. The sequence of the flow layers is altered to explore the influence of reservoir architecture on the results. The reservoir part has a thickness of 150 m and is comprised of three layers with equal thickness and variable flow properties. Basement and overburden impermeable layers with a minimum thickness of 250 m provide conductive recharge to the reservoir. A range of design (well spacing and placement), physical (layered reservoir, fault flow properties, fault throw), as well as operational (injection and production flow rates) parameters are considered in the analysis. All parameter combinations are simulated for an exploitation period of 100 years.

The cold front breakthrough is monitored and its effect on production temperature decline is taken into account for the evaluation of the system lifetime. The total produced energy and the Net Present Value (NPV) are examined at the time of thermal breakthrough. The recovery of the initial Heat In Place (HIP) within the subdomain area is also examined. The insights from this analysis improve the understanding of interdependencies between design, physical and operational parameters with respect to produced energy and economic output. Results from the synthetic models can serve as guidelines to constrain the considered options in full scale field models.

2. Methods

The aim of the study is to identify factors that can affect the system lifetime, the economic performance and the HIP recovery of a geothermal system consisting of a single doublet within a faulted block. It is pertinent to be able to assess the impact of faults as their presence might not be always known prior to development, either due to subseismic imaging resolution, availability of only 2D seismic data or due to the absence of seismic data altogether.

A number of different parameters are considered, in order to have a systematic overview of the interdependencies. This overview is valuable when deciding on development strategies at the field scale. Design parameters such as well spacing and positioning, the fault type and fault throw provide a range of system geometries; physical parameters such as flow properties of reservoir layers and faults can create a wide range of reservoir architectures. Combining the design with the physical parameters enables capturing a multitude of juxtapositions in terms of possible fluid flow paths and sources/sinks of flow. The flow rate effect showcases how the system behaves at different intensities of exploitation. To show how all these effects interact, a full factorial design is performed comprising 2430 unique 3D reservoir simulations.

2.1. Design and inputs

The reservoir is comprised of three layers, 50 m thick each. These dimensions are meant to capture an abstraction of reservoirs considered as geothermal targets in the Netherlands. The reservoir is confined between overburden and basement layers that exhibit very low porosity and permeability (Table 1), equivalent to impermeable rocks. The inclusion of an overburden and basement layer in the model is important as their thermal properties can have a significant effect on the produced energy (Daniilidis and Herber, 2016), and the thermal recharge can affect the system lifetime (Saeid and Barends, 2009). These confining layers have a thickness of at least 250 m to ensure sufficient thermal recharge over the simulation duration of 100 years.

The model includes a doublet positioned in a block that is bounded by two faults. The width of the central block is fixed to 800 m while the spacing of the wells is varied between 600 m and 1000 m. The wells are aligned parallel to faults. The fault plane itself has a thickness of 10 m; this thickness is always outside of the central block. The two faults have an offset that is controlled by the type of faulting and the specified fault throw (see also Table 2 and Fig. 1). The fault throw takes values of 50 m, 75 m and 150 m. Respectively, these represent: bringing two consecutive reservoir layers aligned across the fault surface, having an overlap between two layers on each side of the fault and having a complete disconnection of the reservoir layers across the fault surface. The fault throw is always the same for both faults, regardless of the faulting type. Three faulting types are considered, namely series, graben and horst (Fig. 1).

Due to the fact that the graben and horst faulting types result in a symmetrical model, the doublet positioning for these two fault types is only varying between middle and 50 m away from the west fault (W50). For the fault type in series, the doublet is positioned 50 m away from

Table 2
The input parameters considered in the analysis. All parameter combinations are considered in an experimental design that results in a dataset of 2430 simulations.

Parameter	
Well Spacing (m)	1000, 800, 600
Fault Permeability (m^2)	Sealing (9.86×10^{-18}), Transparent (4.93×10^{-13}), Conduit (9.86×10^{-13})
Fault Throw (m)	50, 75, 150
Fault Type	Series, Graben, Horst
Reservoir architecture	min/mid/max, max/min/mid, min/max/mid
Flow rate (m^3/h)	100, 400
Doublet Position (m)	W50, W100, W200, center, E200, E100, E50

Table 1
The physical properties of the model components. The reservoir, over and underburden layers have a vertical permeability an order of magnitude lower that the horizontal. The fault permeability is assigned to the normal to its plane, while along the fault plane the permeability is an order of magnitude higher. The fault permeability values are determined by the inputs from Table 2.

	Porosity (%)	Permeability (m^2)	Thermal conductivity (W/(m·K))	Specific heat capacity (J/(kg·K)	Density (kg/m^3)
max	20	4.93×10^{-13}	2.9	970	2200
mid		9.87×10^{-14}			
min		$4.93 \times 10_{-15}$			
Fault	20	Fault plane: kFault × 10 Normal to fault plane: kFault	2.9	970	2200
Overburden and basement	1	9.86×10^{-18}	2.2	1100	2400

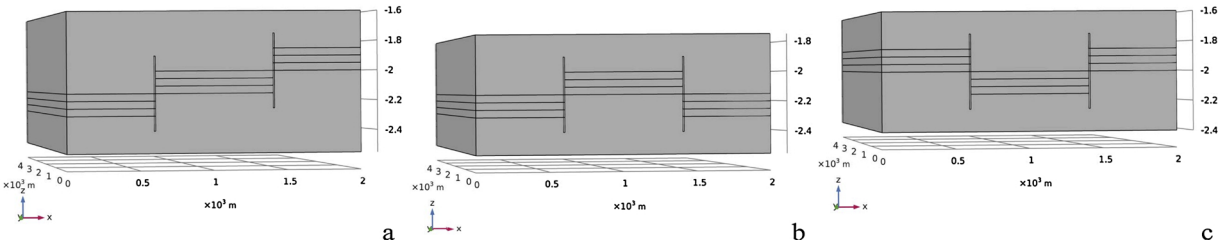

Fig. 1. Model geometries for the different fault types: (a) series, (b) horst and (c) graben. The horst and graben fault types result in a symmetric geometry while the series type of fault in an asymmetric one. The faults always extend 100 m above or below the respective layers they intersect. Here a fault throw of 150 m is shown for all three cases. All axes units are in 10^3 m.

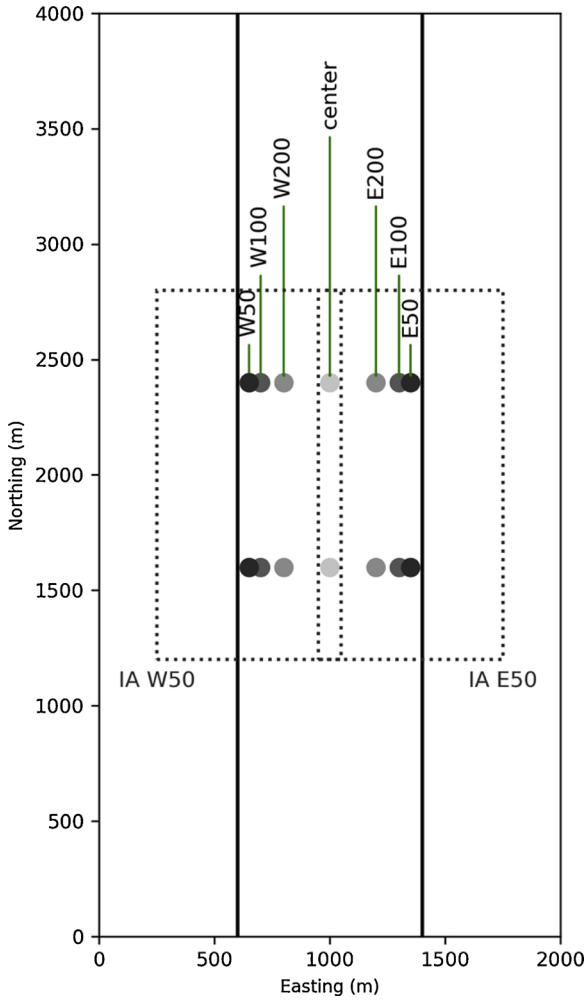

Fig. 2. Positioning of the doublet with respect to the east and west fault, shown here for a well spacing of 800 m. The injector is always positioned in the north and the producer in the south. The Influence Area (IA) of the two extreme positions (W50, E50) is highlighted with a dotted line. The positions are listed in Table 2.

the west fault (W50) up to 50 m away from the east fault (E50) assuming all positions listed in Table 2. A visual representation of the doublet positions and the respective influence area is depicted in Fig. 2.

The top of the reservoir in the central block is always positioned at 2 km depth. A subdomain area is assigned with dimensions of the well spacing by two times the well spacing, as shown in Fig. 3.

The properties of the different model layers are listed in Table 2. The reservoir architecture is represented by alternating the sequence of the three reservoir layers and their respective flow properties. The reservoir layers exhibit the same porosity but their permeability takes one of the discrete values: max (4.93×10^{-13} m^2), mid (9.87×10^{-13} m^2) and min (4.93×10^{-15} m^2). Reservoir permeability is isotropic on the horizontal plane, while the vertical permeability is an order of magnitude lower.

The fault permeability of the normal to the fault plane is an order of magnitude lower than along the fault plane (Tables 1 and 2), the latter is isotropic. Fault permeability takes three values: i) sealing, which is three orders of magnitude lower than the min layer of the reservoir and the same as the overburden and basement confining layers, ii) transparent, which is the same as the max reservoir layer and can be seen as only examining the impact of fault displacement and iii) conduit, which is two times higher than the max reservoir layer. The fault and reservoir layers have the same values of thermal conductivity and specific heat capacity. Porosity and permeability is the same for overburden and basement layers (1 % and 9.86×10^{-18} m^2 respectively).

The well diameter is 21.59 cm (8.5″) for the low flow rate case of 100 m^3/h and 25.4 cm (10″) for the high flow rate case of 400 m^3/h. Table 3 summarizes the input used for the NPV calculations.

2.2. Reservoir model

A Thermal-Hydraulic (TH) model is built in COMSOL Multiphysics. The simulator is selected as a simulator due to its ability to accurately model all relevant physics processes, its flexibility in defining and adjusting the system geometry and controlling the mesh quality using a single software. Simulators that are specifically developed for subsurface fluid flow might yield shorter simulation time. However, for the scope of our studies the utility of the chosen simulator was deemed valuable, together with its flexibility in utilizing multicore systems for embarrassingly parallel problems (i.e. that benefit linearly with the number of available computing resources).

The Energy Balance describes the heat transfer in the model as follows:

$$\rho C\frac{\partial T}{\partial t} + \rho_f C_f \mathrm{q}\nabla T - \nabla(\lambda \nabla T) = 0 \quad (1)$$

in which T (K) is the temperature, ρ the mass density (kg/m^3), C (J/(kg K)) the specific heat capacity, λ (W/(m K)) the thermal conductivity, q (m/s) the Darcy velocity and suffixes $_f$ and $_s$ refer to the fluid and the solid matrix respectively. The thermal conductivity and volumetric heat capacity of the system is computed based on the respective fluid and rock values separately according to:

$$\lambda = (1-\varphi)\lambda_s + \varphi\lambda_f \quad (2)$$

and

$$\rho C = (1-\varphi)\rho_s C_s + \varphi\rho_f C_f \quad (3)$$

in which φ is rock porosity. The pressure field is computed based on the continuity equation according to:

$$\varphi\frac{\partial \rho_f}{\partial t} + \nabla.(\rho_f \mathrm{q}) = 0 \quad (4)$$

where the flux q (m/s) is defined by Darcy's law:

$$q = -\frac{k}{\mu}(\nabla P - \rho_f g \nabla z) \quad (5)$$

in which k is the intrinsic porous medium permeability (m^2), μ the dynamic viscosity of the fluid (Pa·s), g the acceleration of gravity (m/s^2) and P the hydraulic pressure (Pa).

The fluid density and viscosity are a function of temperature according to:

$$\rho_f = 838.466135 + 1.40050603\,T - 0.0030112376T^2 + 3.71822313 \times 10^{-7}T^3 \quad (6)$$

$$\mu = 1.3799566804 - 0.021224019151\,T + 1.3604562827 \times 10^{-4}T^2 - 4.6454090319 \times 10^{-7}T^3 + 8.9042735735 \times 10^{-10}T^4 - 9.0790692686 \times 10^{-13}T^5 + 3.8457331488 \times 10^{-16}T^6 \quad (7)$$

flow rate control on the wells. The well rate is partitioned to each layer based on the ratio of the *kh* (permeability-thickness) of each layer to the *kh* of the whole reservoir interval as formulated in (Jalali et al., 2016) :

$$q_i = \left(k_i h_i / \sum_1^n k_i h_i\right) q_{total} \quad (8)$$

in which k_i (m^2) and h_i (m) are the permeability and thickness of layer $_i$ respectively, $_n$ is the total number of layers and q_i and q_{total} are the layer $_i$ flow rate and the total flow rate respectively.

2.4. Initial and boundary conditions

A geothermal gradient of 31 °C/km (Bonté et al., 2012) and a hydrostatic pressure gradient of 10 MPa/km are applied as initial conditions to the whole model domain. A pressure boundary condition is applied to the sides of the model, equal to the initial values calculated through the hydrostatic pressure gradient.

The model boundary conditions for flow include no flow boundaries on the top and bottom surfaces of the model, while all side boundaries are open to flow. Temperature boundaries include a fixed temperature at the top and bottom of the model according to the initial conditions, while all side boundaries are open to heat transfer.

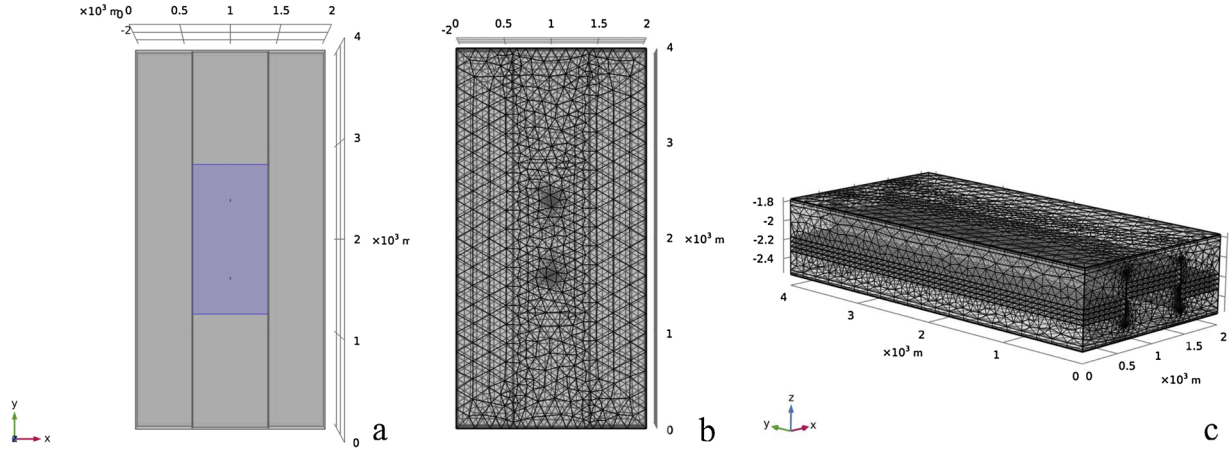

Fig. 3. Subdomain around the doublet (a), shown here for a well spacing of 800 m. The subdomain area has a size of two times the well spacing on the long side and one time the well spacing on the short side. It is considered representative of the expected influence area as considered in the current Dutch licensing scheme for geothermal developments (see also Willems and Nick, 2019). In the event that the subdomain area extends beyond the faults, the corresponding part of the reservoir at that depth is included in the calculation. Example of meshed domain for a horst type of faults in (b) top and (c) angled view. The number of elements ranges between 145k–195k depending on the geometry configuration.

Table 3
Inputs used in the economic calculations.

Load factor (%)	Heat price (€/MWh)	Pump cost (k€)	Pump lifetime (yrs)	Pump efficiency (%)	OpEx % of CapEx (%)	Discount rate (%)	Electricity price (€/MWh)
90	60	500	5	60	5	7	100

The consideration for the mesh was to enable high enough result accuracy while maintaining a reasonable run time for the simulation ensemble. The model is meshed using a higher number of tetrahedral elements inside the reservoir layers, where flow is taking place (Fig. 3a). An additional refinement is performed around the wells where the higher flow velocities occur (Fig. 3b). Moreover, within the subdomain area (see Fig. 3) a further refinement is applied ensuring a minimum of three vertical cells per reservoir layer. The minimum element size inside the reservoir domain is 5 m and the maximum is 70 m. A mesh analysis study was performed to confirm that the chosen mesh sizes provide sufficient accuracy of model results.

2.3. Well model

A simple well model is implemented in order to accommodate a

2.5. Heat In Place (HIP)

The calculation of the Heat In Place (HIP) is carried out according to:

$$HIP = \int_0^{V_{subdomain}} ((\rho_f c_f \varphi + \rho_s c_s (1-\varphi))(T - T_{inj}) dV) \quad (9)$$

The HIP is calculated before any production takes place. The lower bound of the temperature difference is taken as T_{inj} as that is the lowest threshold that can effectively be recovered from the system (Garg and Combs, 2015). The HIP is calculated only inside the subdomain area (Fig. 3).

2.6. System lifetime and NPV

The system lifetime is reached at time t, when the condition for the temperature (°C) of the hot water from the production well is 95 % of the initial production temperature (t = 0)

$$T_{prod_t} \leq 0.95 T_{prod_{t=0}} \quad (10)$$

is met. This condition is quite sensitive and is meant to identify the moment at which a slight change in the production temperature is measured. It therefore can be considered as a worst case scenario for lifetime, bearing in mind that a temperature drop of less than 10 °C may still not compromise the operation of the geothermal system. Nonetheless, such a normalized definition of the production temperature enables cross-comparison between the results. The produced power used for the calculation of income is computed according to:

$$P_{well} = Q \rho_f c_f \Delta T \quad (11)$$

in which Q is the flow rate (m^3/s) and ΔT is the temperature difference between producer and injector wells (°C). The required pump power only considers the pressure drop in the reservoir:

$$P_{pump} = \frac{\Delta P \bullet Q}{\eta} \quad (12)$$

where ΔP is the pressure difference between the wells and η is the pump efficiency. The overall system power is then calculated as:

$$P_{system} = P_{well} - P_{pump} \quad (13)$$

The cost of the wells in € is computed according to (TNO, 2018):

$$C_{well} = 375000 + 1150Z + 0.3Z^2 \quad (14)$$

where Z is the measured depth. For the high flow rate cases that utilize a larger production diameter, the above calculated well cost is increased by 25 %. The NPV is then calculated as:

$$NPV = \sum_{t=0}^{n} \frac{CF_t}{(1+r)^t} \quad (15)$$

Where CF is the cashflow, r the discount rate, n is the project years and t the time. The cumulative produced power generated income is based on the heat price, while the pump power costs are computed based on the electricity price (see Table 3). The NPV and HIP recovery data are selected at the point in time where the system lifetime condition is reached.

3. Results

The results are discussed in an incremental order to arrive at the analysis of the full dataset.

3.1. Cold water front

The shape and extent of the cold water front is affected by the effective flow path that is available based on the simulation input and the flow rate. This flow path is controlled by the reservoir architecture, the fault permeability, the doublet position in relation to the faults, the fault type and throw, the well spacing and finally the flow rate. All combinations of these parameters result in different flow paths and a different special distribution of the cold front. In order to visualize the qualitative behaviour of these interactions, the focus is drawn to a sub-dataset. This sub-dataset uses the higher considered flow rate (400 m^3/h) and highest fault throw (150 m), while the doublet is positioned 50 m away from the west fault (W50) and the fault type is series (Figs. 4 and 5). After 50 years of production the contour line of 1 °C temperature drop exceeds the extents of the outlined influence area regardless of the reservoir architecture and fault flow behaviour (Figs. 4 and 5).

The top view of the middle reservoir layer (Fig. 4) reveals the importance of the reservoir architecture; depending on the flow properties of the middle layer of the reservoir, we can see distinctively different cold water front shapes. The main differences are observed in the extent of the influence area and the volume that is cooled down to the injection temperature of 30 °C. Both the extent and the volume are larger with higher permeability values of the middle layer. Additionally, higher middle layer permeability leads to a more sharply defined edge of the cold plume, owing to the higher Peclet number (i.e. the ratio of heat transfer by advection to heart transfer by thermal conduction) (Fig. 4).

A sealing fault results in a different shape and extent of the cold plume, compared to a transparent or a conduit fault; conduit or transparent fault exhibits very similar pattern of the cold plume (Fig. 4). A sealing fault compartmentalises the reservoir and essentially confined the flow within the faulted block. Proximity to the fault boundary results in a homogeneous development of the cold front along that boundary, as is the case along the west fault (Fig. 4). Between transparent and conduit faults, the shape of the cold plume remains the same for each reservoir architecture, but the extent is reduced for the conduit fault behaviour. This is due to a diversion of large parts of the flow through the fault plane to other parts of the reservoir (see also Fig. 5). While this enhanced flow through the faults can act as a short circuit between the wells (see also section Fault distance, throw and reservoir architecture effect on lifetime) it also enables heat exchange between the deeper sited layers of the western block; this can be seen by the higher temperature flow around the south part of the west fault.

Additionally, a sealing fault exhibits a less widespread temperature diffusion outside its boundaries compared to transparent or conduit properties (Fig. 4). The temperature is lower on the west block for the reservoir architecture that has the maximum flowing layer at the top. This means that right below the depth slice, the highest flow inside the reservoir is present and therefore we observe lower temperatures extending further away from the fault. This effect is also clear in Fig. 5.

The vertical slice presented in Fig. 5 better reveals the interaction between the reservoir layers and the fault plane. With a sealing fault, after 50 years of production the cold plume is limited to the inside of the central block, and heat is only extracted from the surroundings by

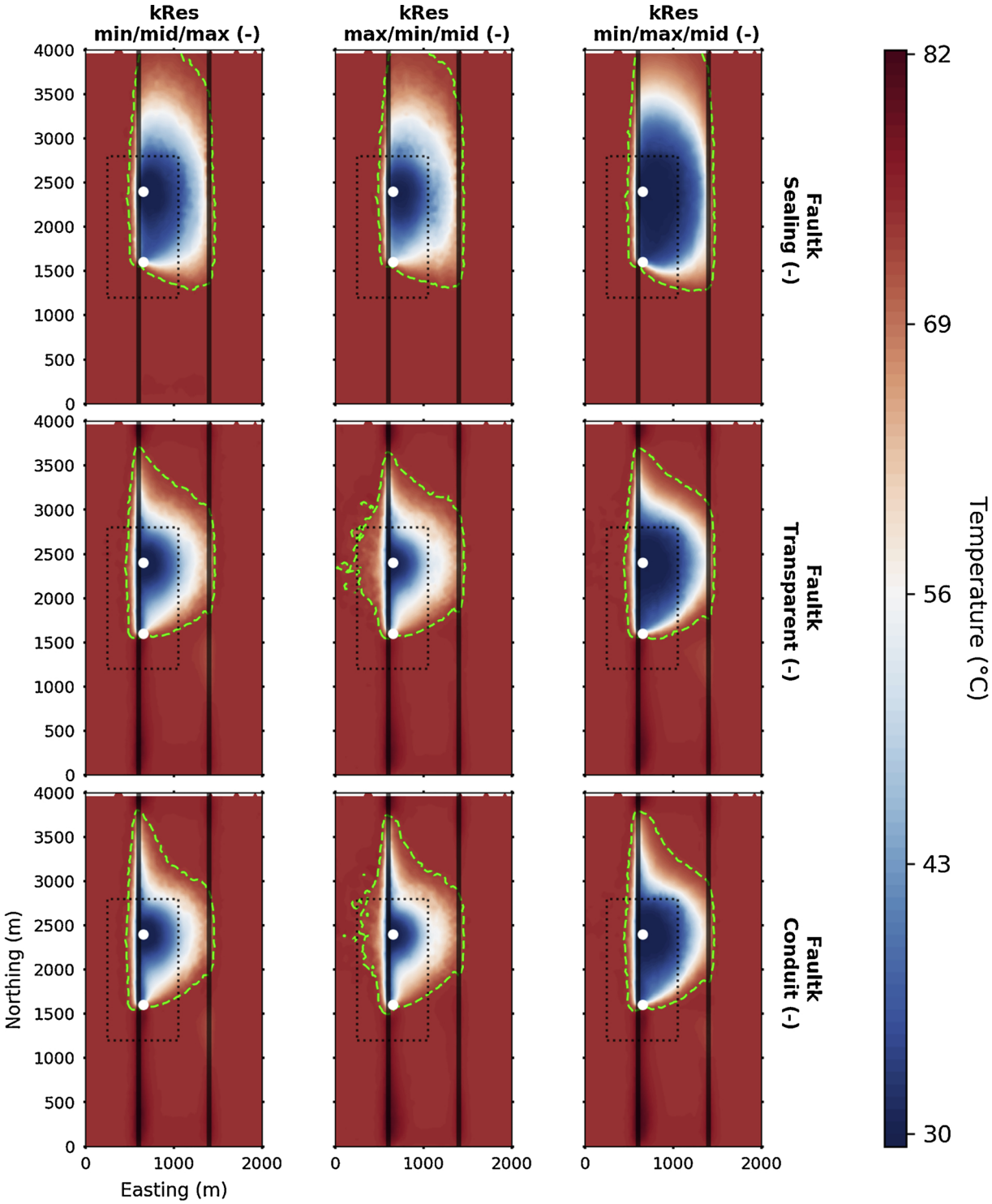

Fig. 4. Cold water front top view, slice at the middle of the reservoir (depth of 2075 m) for the central part of the geometry after 50 years of simulation. White dots mark the injector (North) and producer (South) wells, dark lines mark the faults, the dashed black line marks the extent of the influence area (with size 1 ×well spacing times 2 × well spacing, as described in Fig. 3) and the lime contour represents the extent of a 1 °C temperature drop with respect to the initial conditions (time t = 0). Data shown here for the subset where WSpacing is 800 m, FaultThrow is 150 m, Fault type is series, flow rate is 400 m^3/h and the doublet is positioned 50 m away from the west fault. The West and East parts of each subplot do not represent the same reservoir layers as they are offset by the faults.

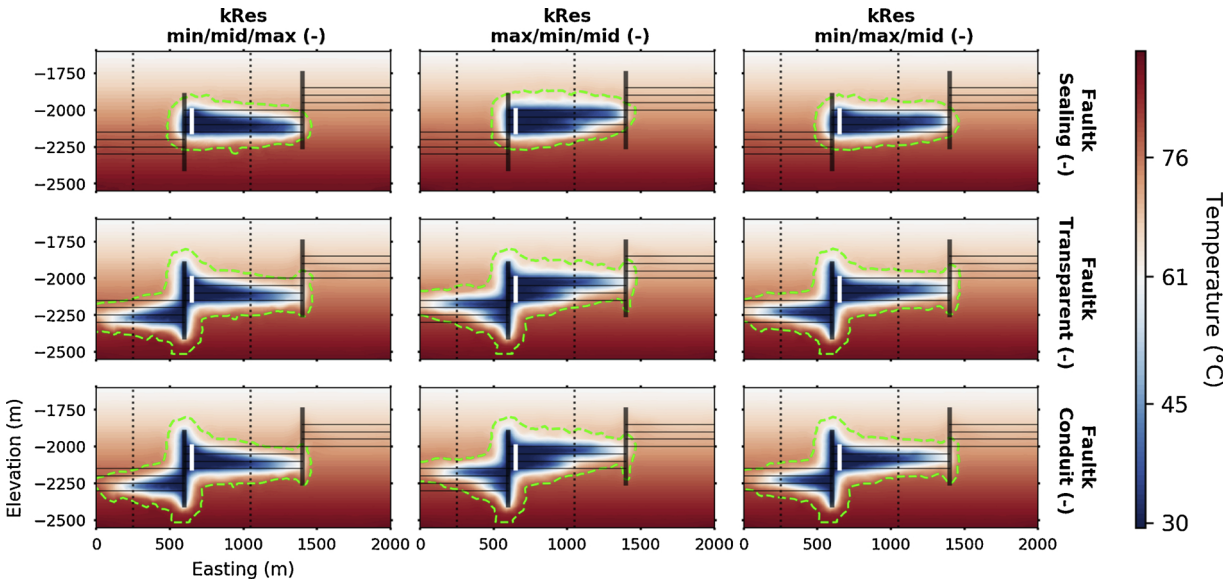

Fig. 5. Cold water front, vertical slice along W-E at the point of the injector well after 50 years of simulation. Horizontal black lines represent the reservoir layer contacts, vertical black lines represent the faults, the vertical white line represents the injection well, the dashed black line marks the lateral extent of the influence area (with size 1 ×well spacing times 2 × well spacing, as described in Fig. 3) and the lime contour represents the extent of a 1 °C temperature drop with respect to the initial conditions (time t = 0). Data shown here for the subset where well spacing is 800 m, fault throw is 150 m, Fault type is series, flow rate is 400 m^3/h and the doublet is positioned 50 m away from the west fault.

conduction. This is clearly demonstrated by the fact that temperature interaction across the west fault only happens at the depth of the central block reservoir layers. With a transparent and conduit flow the cold water also flows along the fault plane and we observe a temperature drop around the whole height of the fault, extending beyond all production layers. After crossing the fault plane, the cold water preferentially flows in the highest permeable layer it encounters (Fig. 5). The lateral extents of the influence area are exceeded after 50 years only towards the east for a sealing fault and both towards east and west for transparent and conduit fault flow properties.

Additionally, Fig. 5 allows for the identification of the different flow layers by means of their respective cold water plume extent. Interestingly, when the minimum flow layer is situated in the middle, we see that despite the flow across the layer boundaries (vertical permeability is an order of magnitude lower) and the heat extraction through conduction, the middle layer cold water front remains recessed (see also section Lifetime and NPV). Lastly, even though not very pronounced, a difference in the extent of the cold water front inside the reservoir layers is observable between the transparent and conduit faults. As discussed previously, this can be attributed to the diversion of a larger part of the flow through the fault and to other parts of the reservoir for the case of a conduit fault.

3.2. Fault distance, throw and reservoir architecture effect on lifetime

For the effect of the fault distance we consider the dataset with well spacing of 800 m and a flow rate of 400 m^3/h, as used in all three figures (Figs. 6, 7 and Fig. A1). For the series type of faulting (Fig. 6) and sealing fault the impact of reservoir architecture is obvious; having the minimum layer in the middle of the reservoir results in higher system lifetime while having the mid and max layers in the middle leads to progressively shorter lifetimes. Even though the max layer is the shallower of the three, the presence of the minimum layer in the middle still leads to the longest system lifetime of all three reservoir architectures. This effect is due to the heat extraction from the middle layer via conduction from both above (max) and below (mid) layers. This effect is further amplified as the fault permeability is increased to transparent and conduit. For a sealing fault there is no significant impact in terms of lifetime with increasing fault throw.

A fault permeability that is at the same order of magnitude as the highest permeable reservoir layer (transparent) introduces an additional, high permeable path through which the cold front can reach the injector (Fig. 6). This in turn leads to a reduction of the system lifetime; this reduction is further exaggerated the closer the doublet is positioned to the fault plane. This finding is consistent for both west and east faults.

For a transparent and conduit fault, as the doublet is positioned closer to the west fault, the decrease of lifetime is less than when the doublet is positioned closer to the east fault (Fig. 6). This is consistent with the west fault block always being situated deeper than the one in the east. Therefore, the fluid and temperature flow that is contributed from the west block is of higher temperature compared to the one from

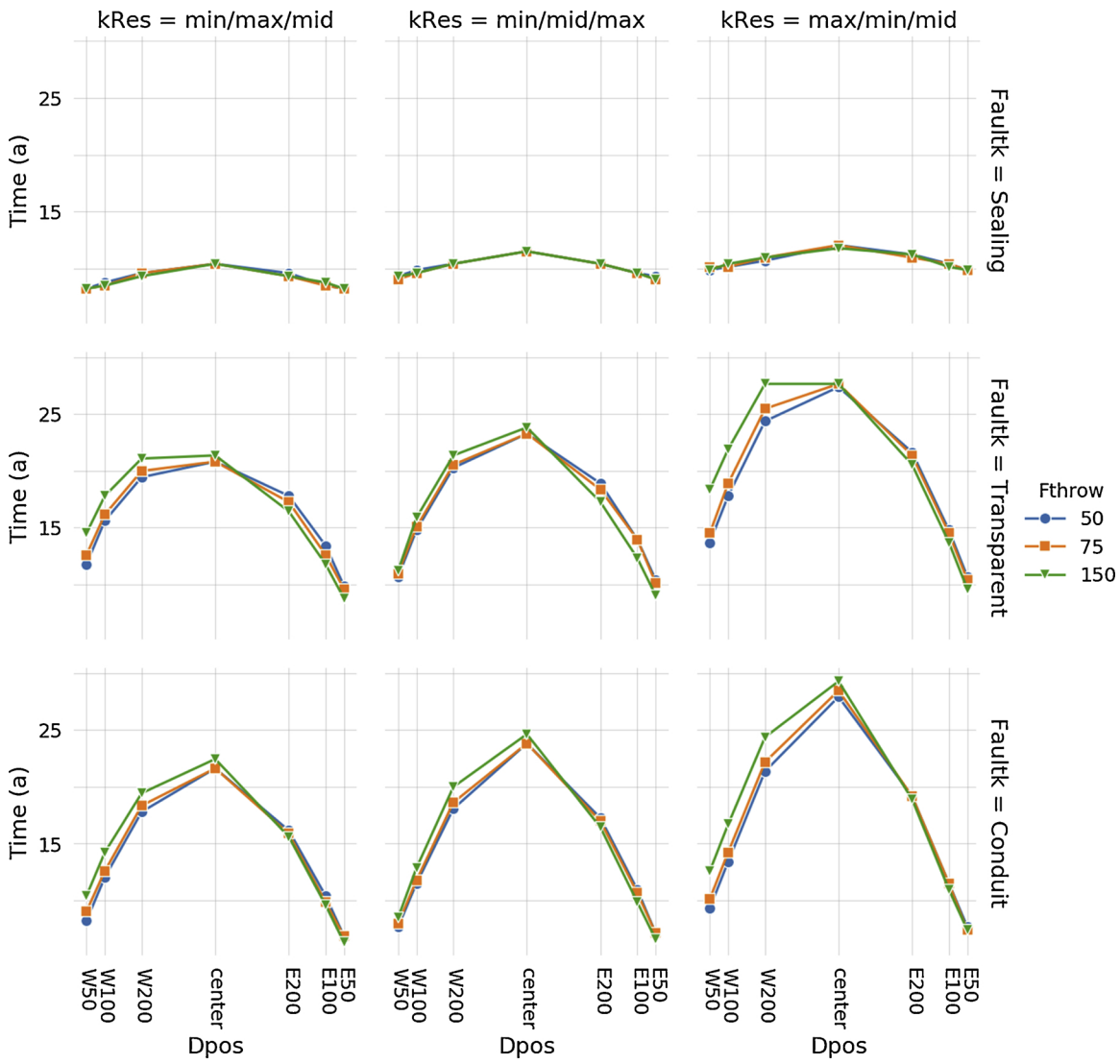

Fig. 6. Effect of fault permeability (rows), reservoir architecture (columns), doublet distance to fault (x axis) and fault throw(colour) on the system lifetime (y axis) for the series fault type. A well spacing of 800 m is used for all data points. The system lifetime criterion is defined in section System lifetime and NPV.

the east.

For a transparent fault, a large fault throw of 150 m (equal to the reservoir thickness) has a smaller negative effect on the system lifetime than a small one of 50 m when moving towards the west fault (Fig. 6). This effect is inverted when the doublet is closer to the east fault.

The largest differences can be observed at the central positioning of the doublet, where the lifetime increases with increasing fault permeability (Fig. 6). This is due to the faults diverting part of the cold water front away from the producer, therefore allowing the production temperature to remain higher for longer periods of time. Overall, moving closer to the fault results in a lifetime reduction of circa 20 % for a sealing fault, to circa 50 % for transparent and conduit faults alike.

Introducing the well spacing as the varying parameter and removing the fault throw as a variable, the qualitative points made in Fig. 6 are amplified or dampened (Fig. 7). Increasing the well spacing to 1000 m extends the system lifetime when the doublet is positioned at the center of the block; at the same time the effect of moving the doublet 50 m away from the fault reduces the lifetime by circa 60 %. The opposite effect can be observed for reducing the well spacing; with 600 m between the injector and the producer, up to 200 m away from the fault on either side has minor effects on the system lifetime. A comprehensive overview of the dependencies is depicted in Fig. 8.

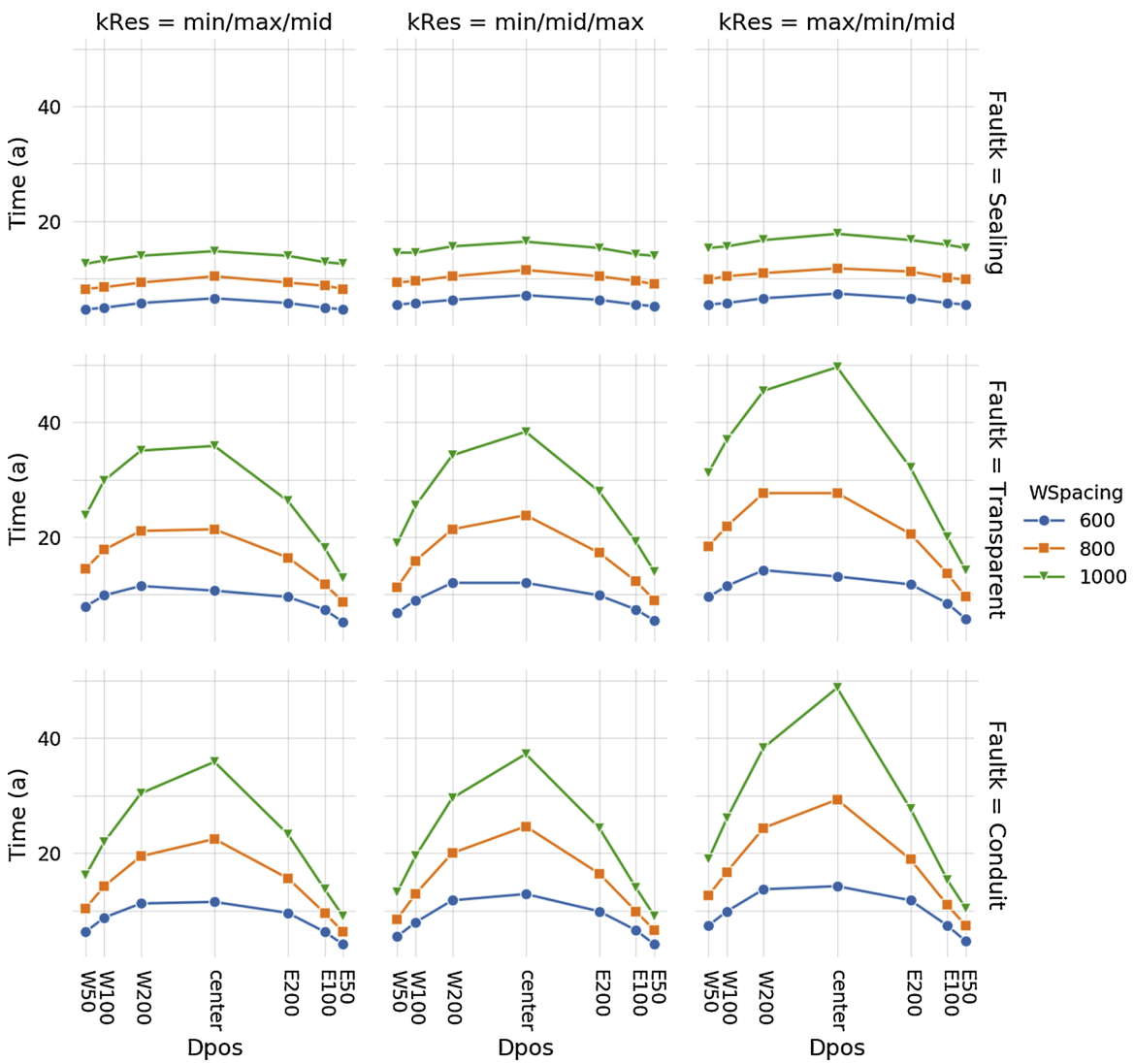

Fig. 7. Effect of fault permeability (rows), reservoir architecture (columns), doublet distance to fault (x axis) and well spacing (colour) on the system lifetime (yaxis) for the series fault type. A fault throw of 150 m is used for all data points. The system lifetime criterion is defined in section System lifetime and NPV.

3.3. Lifetime and NPV

3.3.1. NPV and flow rate

Examining the full dataset of 2430 simulations, higher NPV values (computed at the lifetime point) are achieved for an injection and production flow rate of 400 m^3/h compared to the lower one of 100 m^3/h (Fig. 9). Nonetheless, the COP is decreased when higher flow rates are used, even though a wider well diameter is in place (see section Design and inputs). A reduction of the COP does not seem to affect the NPV as the values are increased for higher flow rates. For the high flow rate there is a good correlation between the system lifetime and NPV; when the former is longer the latter is increased. This correlation is not as straightforward for the low flow rates, indicating that other parameters influence the NPV (see section NPV overview). Additionally, the highest achieved NPVs for the low flow rate case are comparable to the lowest achieved NPVs for the high flow rates. Overall, there seems to be no clear pattern with regards to the generated NPV and COP for the considered model and input range.

Examining the NPV values against the cumulative produced energy (a proxy for the system lifetime) clarifies the trend further; both datasets exhibit a logarithmic type of behaviour (Fig. 10). For the low flow rate the data points are more scattered, meaning that other parameters also influence mostly the generated NPV, as multiple NPV values are encountered for similar amounts of cumulatively produced energy. On the other hand, the high flow rate dataset exhibits much less scatter of the data points, implying, as discussed before, that the effect of the high flow rate is decreasing the significance of the other parameters. For both flow rates there is a levelling off in terms of NPV, meaning that a longer lifetime would not yield higher economic value. Nonetheless, it is clear that for the reservoir properties considered, increasing the flow rate four times results in an increase of NPV of a factor seven. This suggests that if the reservoir architecture and permeability are suitable it is favourable to increase the flow rates.

3.3.2. NPV overview

The impact of the doublet position to the changes in NPV is depicted in (Fig. 11). For the dataset shown in Fig. 11, positioning the doubler at least 200 m away from a fault would avoid losses larger than circa 20 % in the generated NPV. For a sealing fault changing the doublet position from the center of the block leads to NPV losses; these losses amplify as

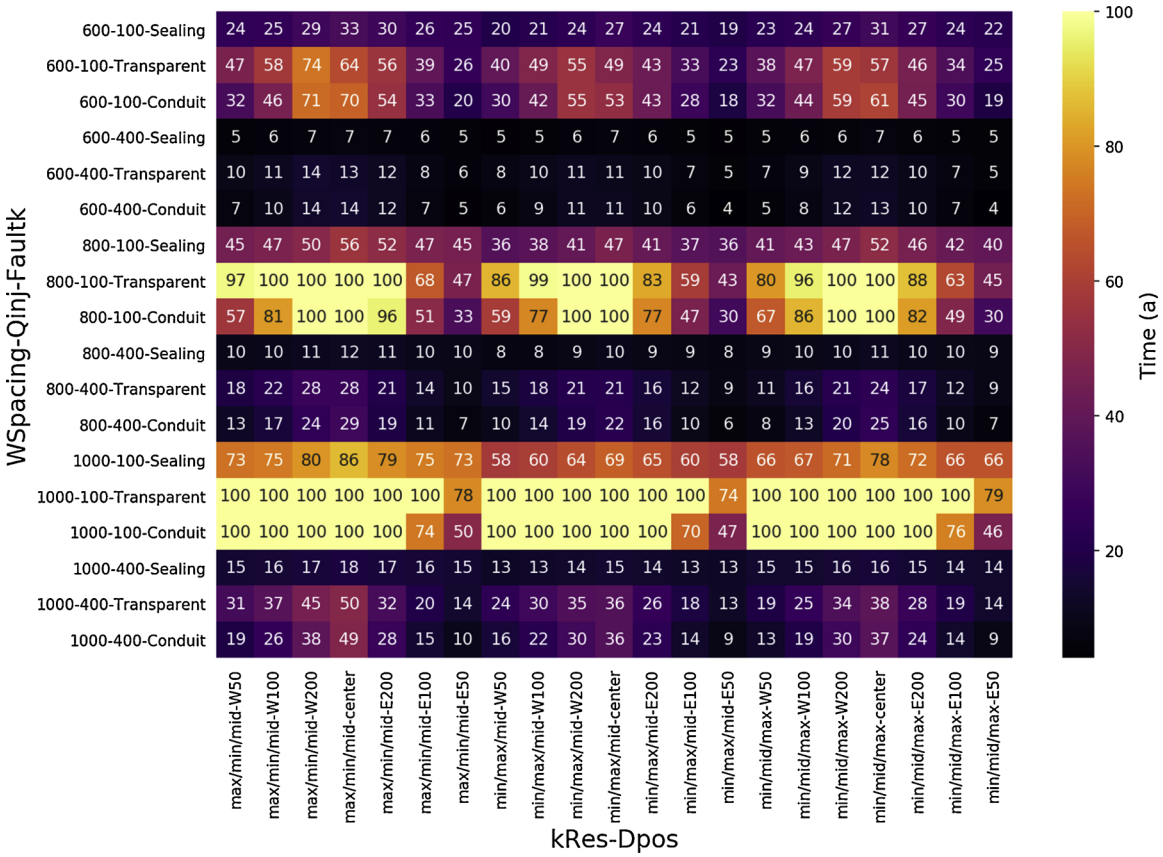

Fig. 8. Heatmap plot of the systems lifetime for all the combinations of reservoir architecture and doublet position (x axis) against all the combinations of well spacing, injection flow rate and fault permeability (yaxis).

the well spacing decreases for both the high and low flow rates. For both a transparent and a conduit fault the polarity of the fault offset becomes important. Positioning the doublet closer to the east fault leads to NPV loses; these loss increases the closer the doublet is positioned to the east fault. This observation is consistent for both low and high flow rates, with higher flow rates further amplifying the percentage decrease of the NPV. Increasing the fault permeability to conduit further amplifies the effect, especially for the doublet being positioned 50 m away from the east fault. The east block is positioned shallower than the central block and therefore any fluid produced from the east reservoir

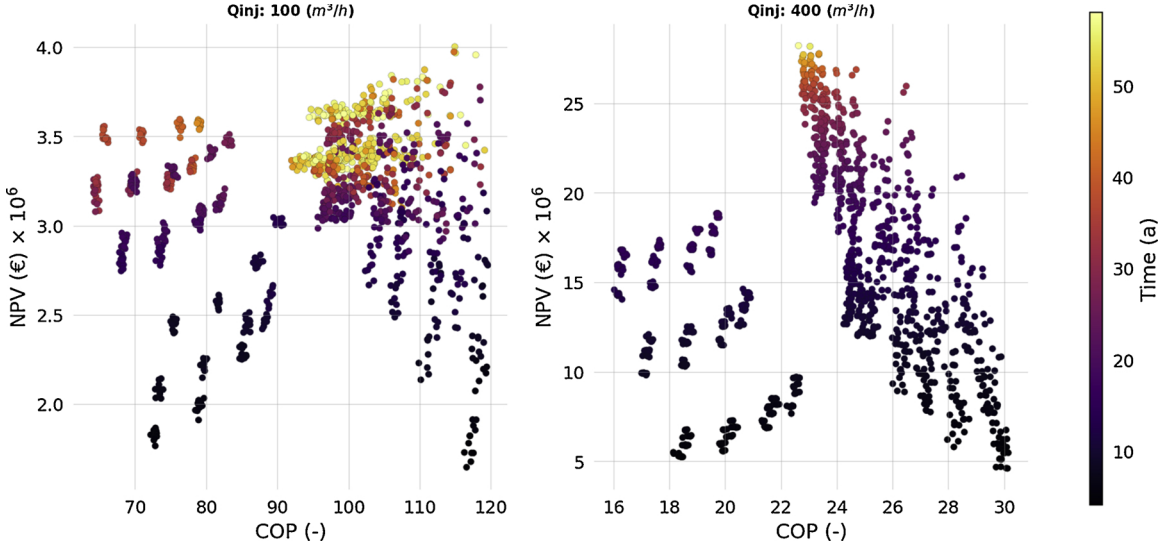

Fig. 9. COP against NPV for the full dataset of 2430 simulations, plotted according to injection/production flow rate and coloured according to the system lifetime.

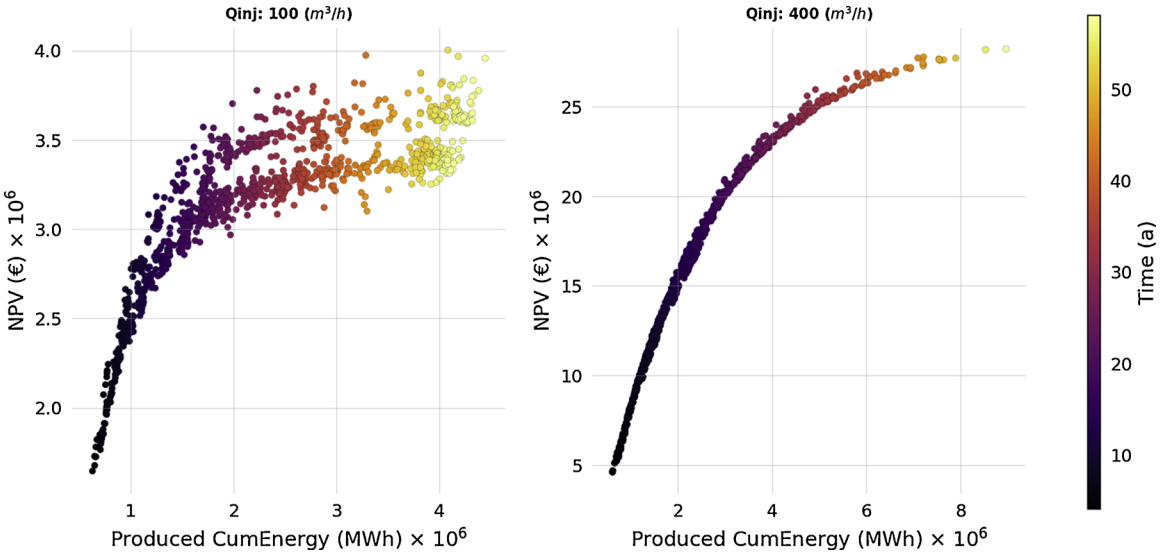

Fig. 10. Gross cumulative produced energy and NPV for the full dataset of 2430 simulations plotted according to injection/production flow rate and coloured according to the system lifetime.

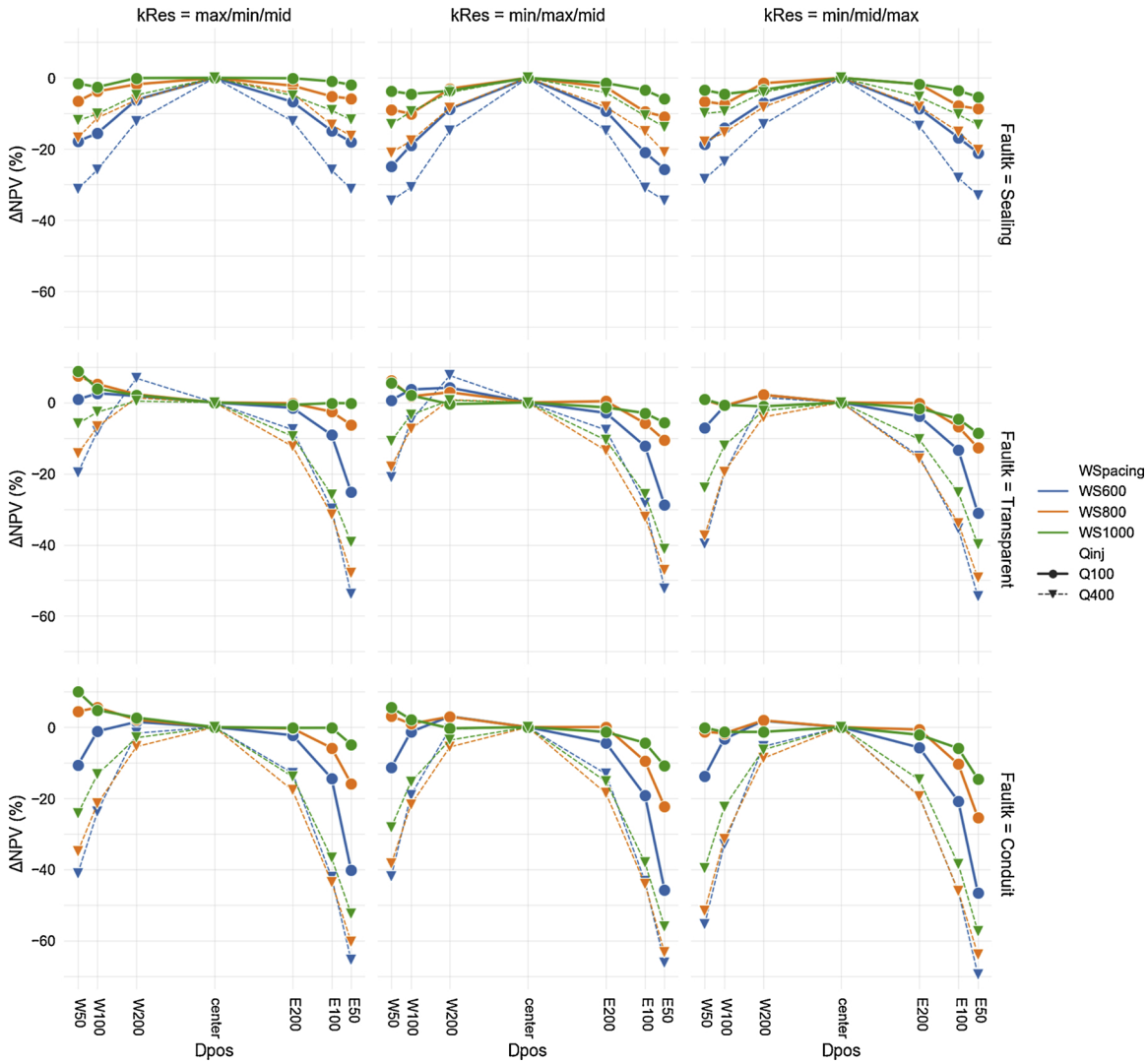

Fig. 11. Changes in NPV (%) (y axis) for different doublet positions in relation to the faults (x axis), different fault permeability (rows) and different reservoir architectures (columns) for the subset of data with a series fault type and fault throw of 150 m. The data are colour coded according to the well spacing and different flow rates are indicated by the line style.

part will reduce the production temperature, leading to lower energy generation and possibly earlier thermal breakthrough.

Contrary to this, positioning the doublet closer to the west fault results in a more complicated effect on the NPV change. For 200 m distance, high flow rates exhibit either a minor increase or no NPV change. Closer than 200 m to the west fault results to an NPV decrease which is more significant for lower well spacing. The reservoir architecture seems to also be important here as having the maximum producing layer at the bottom of the reservoir section yields the largest NPV drop.

For low flow rates different effects are observed. For a transparent fault, a well spacing of 600 m leads to either no NPV effects or minor losses, while for a conduit fault these losses reach up to 10 % decrease of the NPV compared to the doublet being positioned at the center. However, for a well spacing of 800 m or 1000 m there is a slight increase in the NPV that can reach up to 10 % for the reservoir architecture with the minimum flowing layer in the center. A transparent fault has almost the same effect for both well spacing values, but a conduit flow slightly differentiated between the two with the larger well spacing exhibiting higher benefits.

3.4. Energy recovery

Energy recovery as a function of system lifetime gives an indication of the rate of recovery within the defined subdomain boundaries. For the whole dataset the HIP recovery does not fall below circa 10 % under any parameter combination. For low flow rates the recovery never exceeds 50 %, whereas for high flow rates it only exceeds 50 % in very few cases (Fig. 12). Nonetheless, a clear clustering is observed for both flow rates: the combination of well spacing and fault behaviour controls the ratio of HIP recovery to system lifetime.

For the low flow rate of 100 m^3/h a higher separation can be seen between the different well spacing clusters in terms of system lifetime, while for the high flow rate of 400 m^3/h the well spacing clusters are closer together. A higher flow rate leads to a comparable heat recovery values with the low flow rate, but this is achieved in a shorter system lifetime. The small decrease in terms of recovered HIP between the high and low flow rate could be attributed to lower flow rates sweeping a large part of the reservoir and to high flow rates reaching an earlier thermal breakthrough.

Increasing the fault throw leads to longer system lifetimes for both the high and low flow rate datasets. However, for the high flow rates, a longer lifetime slightly increases the HIP recovery while this is not observed for the low flow rates. Nonetheless, for both flow rates we observe a further separation between the clusters of the well spacing when moving to the largest fault throw of 150 m. This effect is more pronounced for the low flow rate dataset and is further examined in Fig. 13. The factor differentiating the well spacing sub-dataset is the type of faulting; a graben type of fault achieves a lower HIP recovery compared to a horst or series type, with the latter two exhibiting comparable values. This impact however diminishes with increasing well spacing. Lastly, the reservoir architecture with the minimum flowing layer in the middle consistently leads to high HIP recovery.

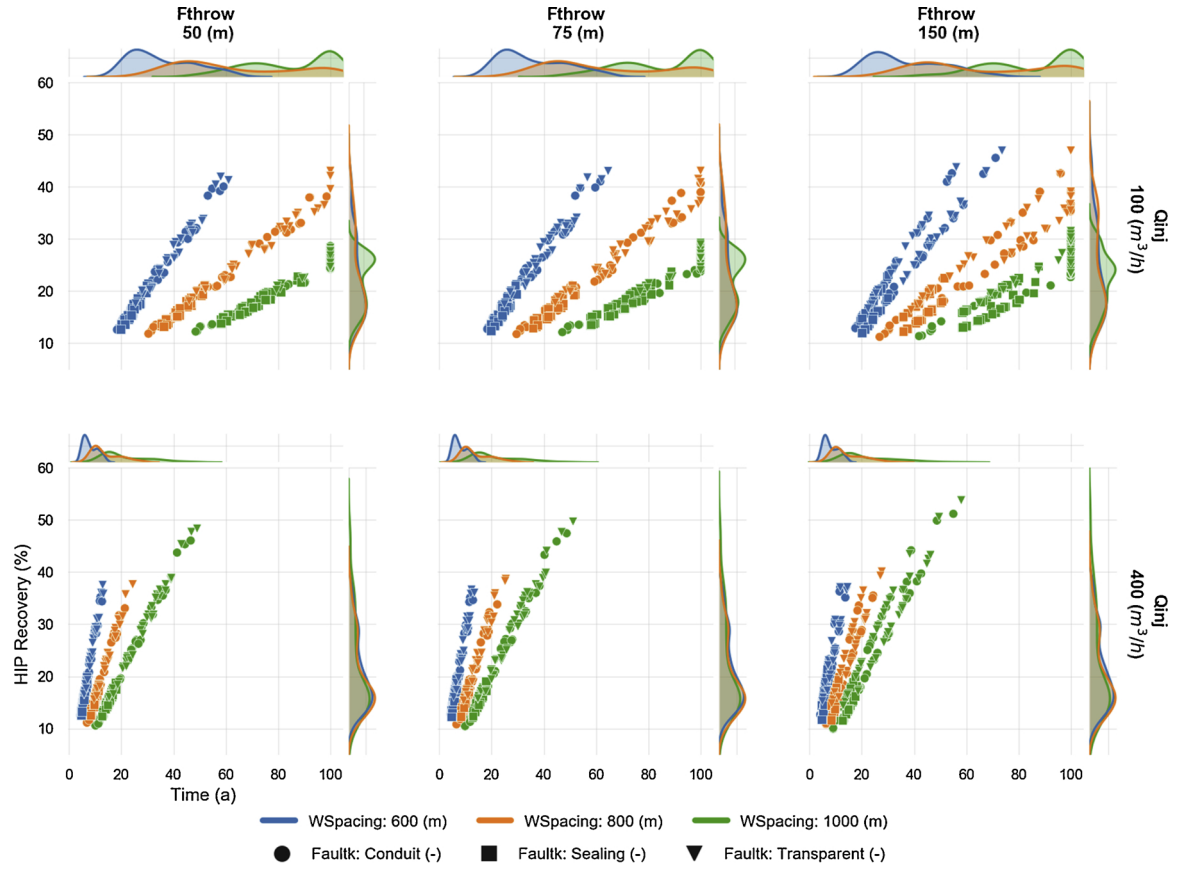

Fig. 12. Percentage of recovered HIP within the subdomain boundaries of the model. Data are coloured according to the well spacing and marked according to the fault permeability.

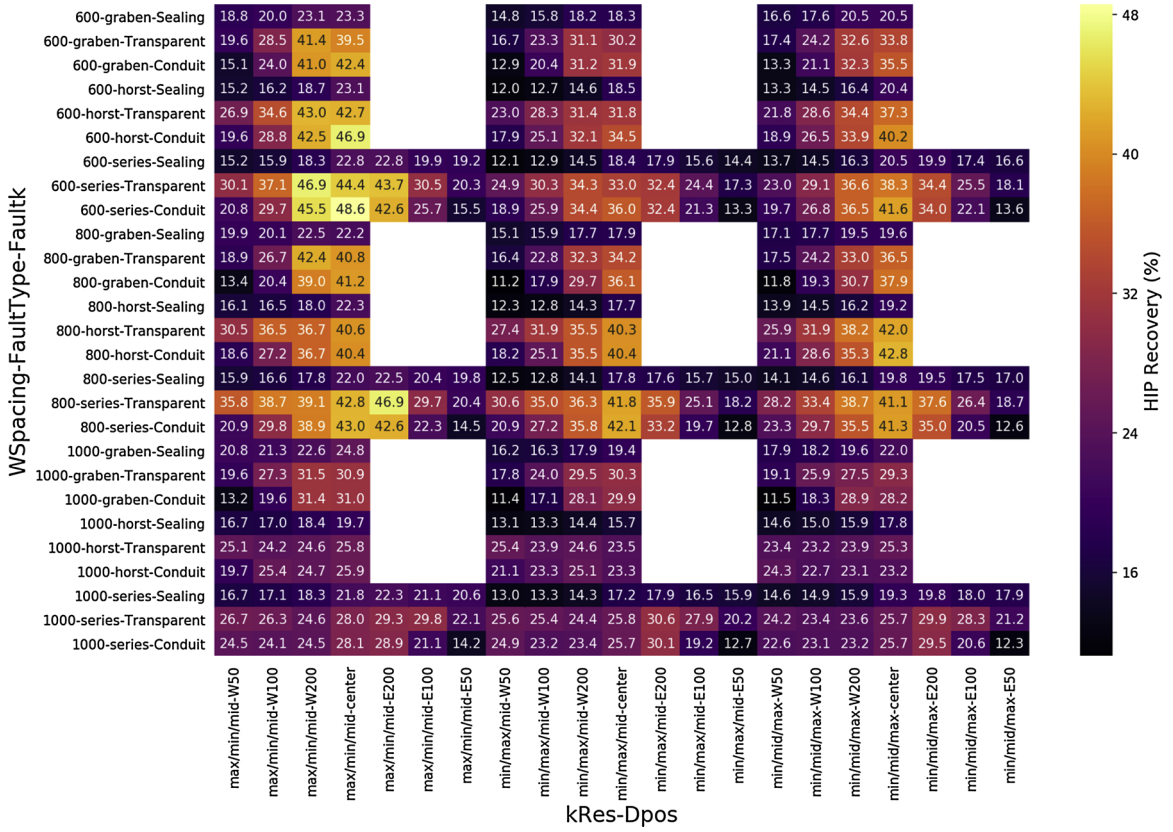

Fig. 13. Heatmap of the HIP recovery (%) for a data subset with a fault throw of 150 m and a flow rate of 100 m3/hr (upper right subplot of Fig. 13).

4. Discussion

The results analysis suggests that fault permeability is more important than fault throw regarding the system lifetime, at least while the fault throw is not larger than the reservoir thickness. Additionally, a smaller well spacing is proportionally less sensitive to the doublet position with respect to the fault, compared to a larger well spacing. For field development this means that an assessment of the fault flow properties is more crucial than being able to better characterize structurally the fault throw. Moreover, if uncertainties regarding the fault flow behaviour cannot be reduced, a development plan utilizing smaller well spacing would minimize any adverse effects of the faults on the system lifetime.

A higher fault throw increases the impact the fault has on system lifetime. In the presence of 3D seismic data fault throws equal to the considered reservoir target should be identifiable; this however might not be the case if only 2D seismic data are present depending on their orientation, or if seismic data are not present at all. Nonetheless, it remains important to identify how the flow inside the fault interacts with the adjacent blocks. Enabling fluid flow and thermal exchange with deeper situated parts of the reservoir can increase system lifetime while the opposite is true for shallower parts. In that sense identifying the vertical relative positions of the blocks is of higher significance compared to the fault throw. This argument is only valid, however, if a possible connection of the fault with other reservoirs that might be above or below the main one and could be connected via the fault is not considered, as in this study. Such a connection would override the findings from the current study and would need to be separately addressed.

The finding that sealing faults resulting in shorter system lifetimes due to an effective reduction of the volume available for heat extraction is consistent with previously presented work in Daniilidis et al., 2016a,b. Blöcher et al. (2010) postulated a possible fault reactivation of a previously no-flow boundary fault as a connecting fluid pathway to explain a faster hydraulic connection between wells, identifying fault structures as important hydraulic elements. This suggestion is in line with the findings of this work with regards to transparent or conduit fault properties. Blöcher et al. (2010) further pointed out that fault pressure dependent conductivity is the most important for further investigations. This aspect while not part of the analysis in this paper has been shown to drastically change the flow behaviour or smaller elements such as fractures in Salimzadeh and Nick (2019). Additionally, Lepillier et al. (2019) showed the dependency of fracture flow behaviour for different matrix rock properties highlighting the permeability contrast between matrix and fractures together with the mechanical properties of the matrix as important factors in predicting flow behaviour. Salimzadeh and Nick (2019) further showed a progressive reduction is production temperature with an increasing density of hydraulically conductive fractures. While fractures are significantly smaller in extent, they can be considered as proxies for the behaviour of larger elements such as faults. Therefore, previously reported results on the permeability contrast between matrix-fractures are in accordance with the findings in this study for main reservoir-fault permeability contrast: with a higher contrast leading to amplified impact on the modelled system lifetime.

The influence area of the doublet, currently considered with dimensions of 1 ×well spacing times 2 × well spacing (Fig. 3), fails to contain the influence of the cold front. This boundary is always exceeded within 50 years by a 1 °C temperature drop with respect to the initial temperature when using high flow rates. As a result the considered shape and dimensions of the influence area could be re-evaluated for licensing purposes. The outline of the cold front does not show a rectangular shape and the fault behaviour adds another differentiating factor to the final shape of the cold plume. This is true for the data shown here, using homogeneous flow properties for the reservoir layers, but is has also been recently shown for heterogeneous systems (Babaei and Nick, 2019). Perhaps a more applicable direction would be to consider a circular area of influence, centred around the injector well with a dimeter at least equal to the well spacing as this would couple it

directly to the interests of the developers with regards to cold front breakthrough. Research towards this direction could yield more concrete argumentation for an improved scheme.

Reservoir architecture is also important to consider, as having the minimum flowing layer between the medium and high flowing layers yields a longer system lifetime. It can therefore be argued that a reservoir with a lower permeability zone in the middle (surrounded by more permeable layers) would be preferable for geothermal production, as it can deliver heat for a longer period due to greater interaction between the low and high permeable layers of the reservoir. Compared to having the largest flow layer at the bottom of the reservoir, which yields a higher producing temperature, a low flowing layer in the middle acts as a heating element to both layers above and below, therefore extending system lifetime. Additionally, two reservoirs separated by an impermeable layer may also exhibit a similar behaviour resulting in a longer system lifetime than one reservoir with the stacked thickness of both reservoirs together, if the temperature difference between the reservoirs is not too high. The use of comparable thickness for all three reservoir layers also implies that extrapolation of the results to layers of different thicknesses or different ratios between the layer thickness may not be valid. This effect of varying layer thickness should still be investigated.

Smaller models as used in this paper can still be used to conceptually capture a certain reservoir architecture. When this is achieved, the shorter simulation time and quantification of the impacts can provide insights that limit the number of options considered in full scale models. The use of homogeneous reservoir properties in all reservoir layers, implies that these results remain valid when lateral permeability variation is limited. Therefore, insights from this analysis are more applicable to alluvial-deltaic, aeolian or otherwise stratified depositional settings with wider lateral extents, compared to strongly channelized fluvial settings (as discussed in e.g. Babaei and Nick, 2019). For such settings further analysis should be performed.

The NPV results suggest that from an operator's perspective the appeal to aim for high flow rates would be very strong. The higher flow rates dataset achieves NPV values that are never lower than the NPV values of the full low flow rates dataset; this holds true despite the shorter system lifetime of the high flow rate cases compared to the low flow rate ones. Increasing the flow rate four times results an NPV increase of about a factor seven for the reservoir properties considered. However, it is important to notice that this relationship might be different if other reservoir properties are in place. Changes in the pressure response of the reservoir to higher flow rates might yield different pressure requirements and consequently NPV values. With regards to doublet positioning with respect to faults, ensuring a distance of at least 200 m would limit the effect of the fault regardless of its flow properties to less than circa 20 % of the NPV generated when the doublet is positioned at the centre of the block. Additionally, high flow rates reduce the impact of other parameters to the generated NPV compared to low flow rates. Nonetheless, the value of the system appears to level off for both high and low flow rates, further reducing any incentive for operators to strive for extending the system lifetime. This finding possibly hints at the presence of an optimum balance between system lifetime and generated value, which, however, is beyond the scope of this paper. It is worthwhile noting that the NPV results shown in this study might be different when considering different economic input (e.g. heat and electricity prices, discount rate, etc) than that mentioned in section System lifetime and NPV. Notwithstanding, using the same input for the whole factorial design enables systematic observations.

Contrary to the results regarding system lifetime, where a shorter well spacing is less affected by the doublet proximity to faults, the NPV generated by larger well spacing proves more resilient to doublet positioning. Even in the event of a cold water shortcut through the fault plane the larger well spacing ensures a long enough lifetime to achieve a higher generated value. Nonetheless, flow rate remains important; increasing the flow rate reduces the differences between the well spacing options and further amplifies the effect of the doublet being positioned closer to the fault plane.

The achieved HIP recovery shows a similar pattern to the NPV results. High flow rates that lead to increased HIP recovery at shorter lifetime suggest operators would be encouraged to pursue this type of development. This remains a pertinent issue to be addressed by regulators in order to ensure the longevity of energy supply for such systems. Moreover, in a densely utilized subsurface space with multiple competing uses (van Os et al., 2016), the growing importance of regional development needs to be highlighted. Recently discussed visions of coordinated doublet development (Willems and Nick, 2019) might need to be enriched with insights from the interplay between structural elements such as faults and development options such as well spacing and positioning.

Lastly, the proximity and interaction of geothermal production to faults might raise issues regarding seismicity. Positioning the doublet up to 50 m away from sealing faults might only reduce the generated NPV by up to circa 30 %. However, the resulting pressure field and lower temperature of the cold front could influence fault stability as previously shown (Jeanne et al., 2017; Kim and Hosseini, 2015). Especially in light of regional developments these concerns should be addressed by ensuring that faults are not rendered unstable via the pressure field of geothermal energy production. While this aspect was beyond the scope of the current study, it is highly relevant to pursue such analysis in the future.

5. Conclusions

This study aims to improve the understanding of interdependencies between physical and operational parameters for direct use geothermal heat. A systematic analysis utilizing a full factorial design is carried out to identify factors that can affect the system lifetime and economic performance of a single doublet within a faulted block. The analysis includes 2430 unique Thermal Hydraulic (TH), 3D reservoir simulations. Considerations of physical parameters include the fault type and fault throw, flow properties of reservoir layers and faults, while operational parameters include well spacing, well positioning and flow rate.

The characterization of fault flow properties is more significant compared to the fault offset. Additionally, system lifetime is less affected by the presence and flow behaviour of faults when a smaller well spacing is utilized. The fault flow properties have a significant impact to the shape and extent of the cold plume and therefore the system lifetime. Faults that enable fluid flow lead to longer thermal breakthrough times since part of the flow is diverted away from reaching the production well. However, the presence of faults that enable fluid flow increases the sensitivity of the doublet positioning to the fault location. Contrary to this, a fault with a sealing behaviour renders the system lifetime less sensitive to the doublet positioning.

Results suggest that operators would always opt for higher flow rates, since the generated NPV using 400 m^3/h is at all times higher than any scenario considered with a lower flow rate of 100 m^3/h. Moreover, increasing the flow rate four times results in an NPV increase of a factor seven for the considered reservoir properties. NPV's of low flow rates are more sensitive to other parameters in absolute terms, while higher flow rates only appear sensitive to system lifetime. For both flow rates the NPV demonstrate an asymptotic behaviour implying that further extension of system lifetime does not yield additional benefits. This finding implies the presence of an optimum in terms of the balance between system lifetime and generated value.

Reservoir architectures with a low flowing layer in the middle, or two individual reservoirs separated by an impermeable layer showcase improved system lifetime and NPV generation. The presence of a less permeable layer in the middle acts as a heating body, leading to improved extraction from the production layers as well as from over- and under- burden bodies. This result is present for both high and low flow rates although it is more pronounced for the former.

The current influence area definition around doublets (1 ×well

spacing times 2 × well spacing) fails to contain the resulting cold water plume. Therefore, an improved definition of the influence area should be developed for monitoring and planning purposes.

Results from the synthetic models shown can serve as guidelines to reducing the considered options in full scale field models. The importance and relevance of these results remains very high for layered reservoirs with good horizontal homogeneity.

Availability of data and materials

The datasets used and/or analysed during the current study are available from the corresponding author on reasonable request.

Funding

This work has been funded by the Dutch Ministry of Economic Affairs and Climate Policy and ECW Netwerk BV under the research program Kennisagenda.

CRediT authorship contribution statement

Alexandros Daniilidis: Conceptualization, Methodology, Software, Formal analysis, Investigation, Resources, Data curation, Writing - original draft, Writing - review & editing, Visualization. **Hamidreza M. Nick:** Conceptualization, Methodology, Writing - review & editing, Supervision, Project administration, Funding acquisition. **David F. Bruhn:** Writing - review & editing, Project administration.

Acknowledgments

The authors would like to acknowledge the constructive feedback of Harmen Mijnlief (TNO), Raymond Godderij (EBN), Bertran de Lange (ECW Netwerk) and Frank Schoof (Platform Geothermie) that helped shaping this work. We are also thankful to the contstructive feedback and comments of our anonnymous reviewers that improved the original manuscript.

Appendix A

Horst and graben fault types (Figs. A1 and A2 respectively) exhibit the same results as the series type faulting validating the influence of the reservoir architecture and the qualitative effects of positioning the doublet closer to the fault.

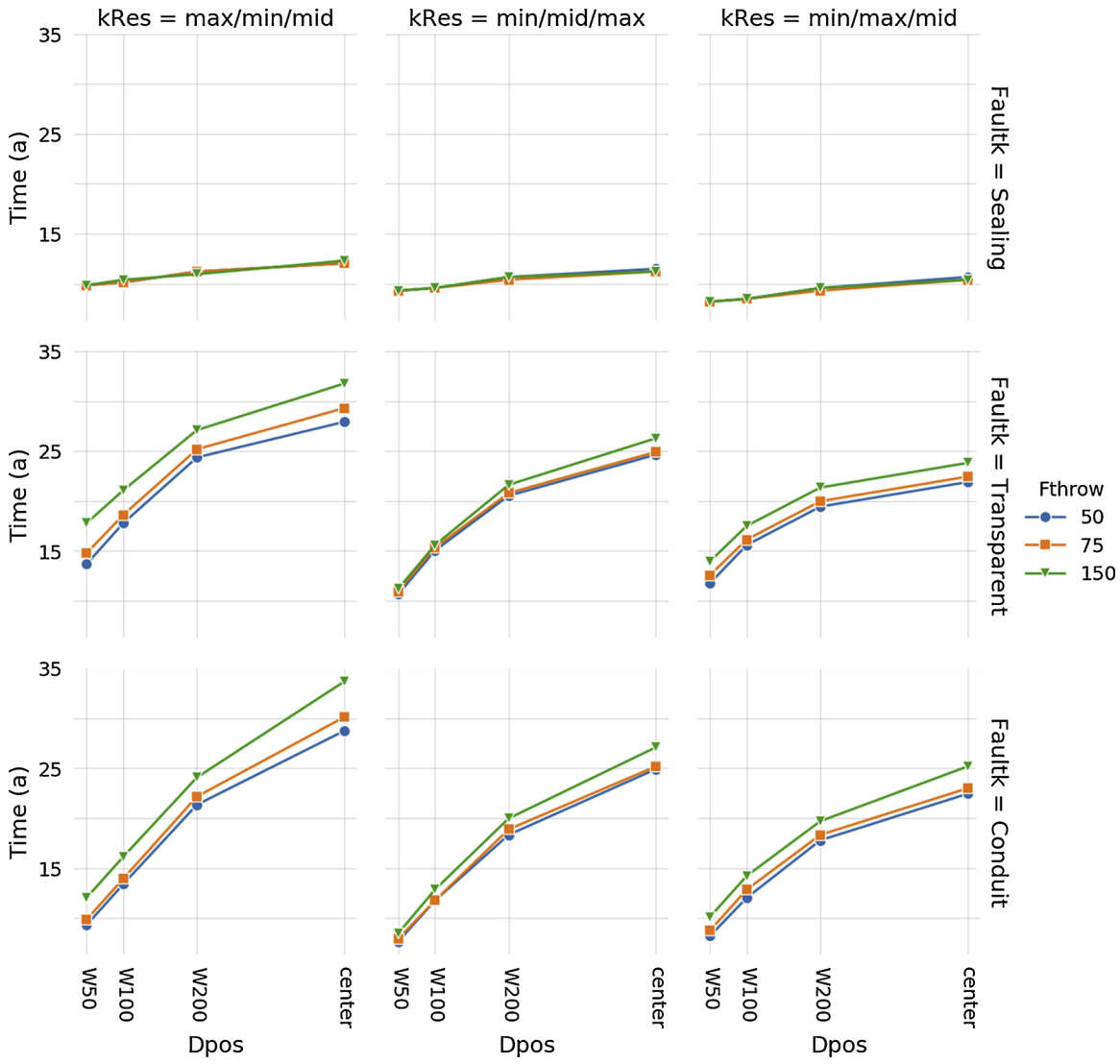

Fig. A1. Effect of fault permeability, reservoir architecture, doublet distance to fault and fault throw on the system lifetime for the horst fault type. A well spacing of 800 m is used for all data points. Both West and East fault blocks are situated deeper compared to the central block, therefore due to symmetry, the doublet is only moved towards the west block. The system lifetime criterion is defined in section System lifetime and NPV.

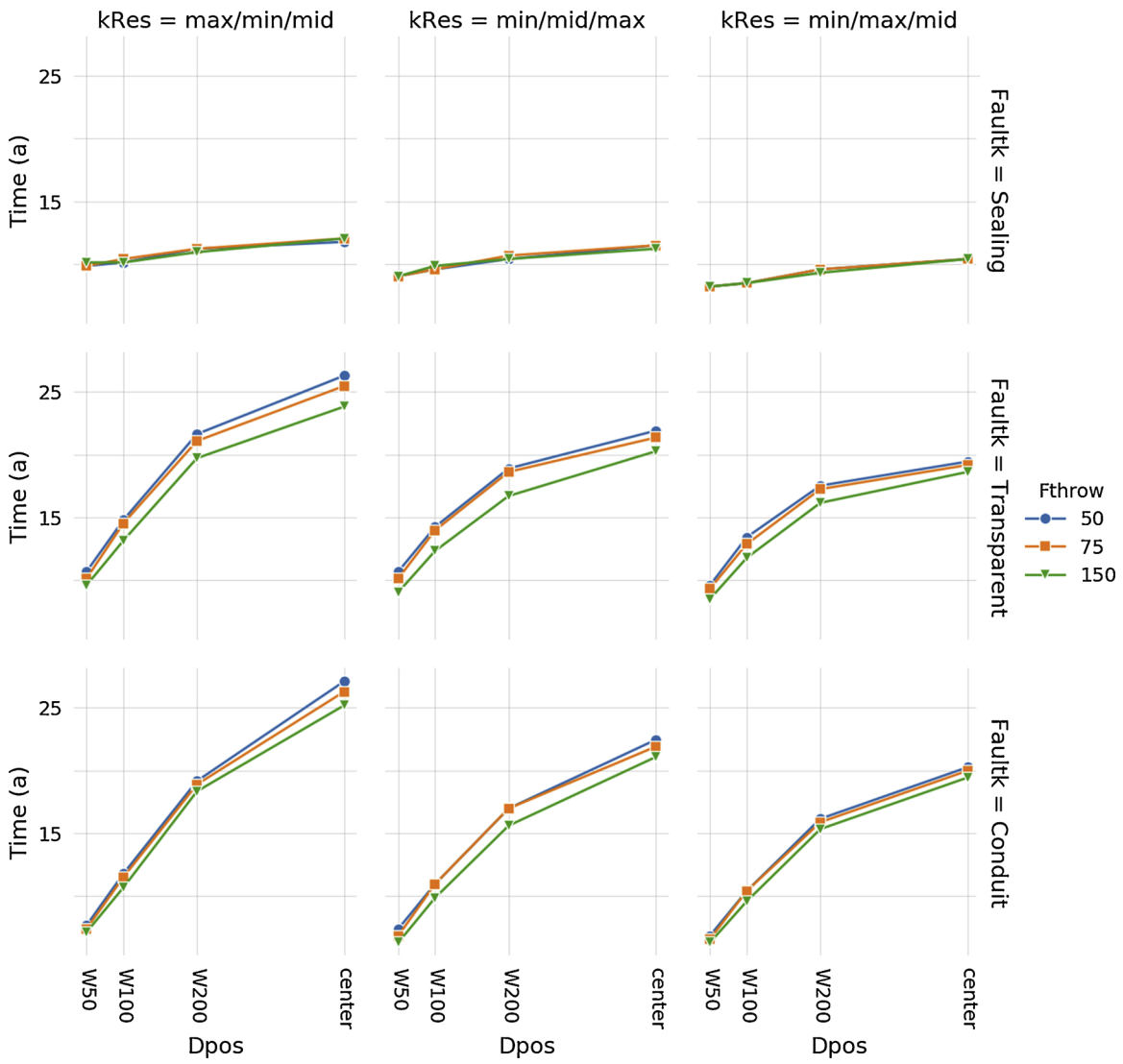

Fig. A2. Effect of fault permeability, reservoir architecture, doublet distance to fault and fault throw on the system lifetime for the graben fault type. A well spacing of 800 m is used for all data points. Both West and East fault blocks are situated shallower compared to the central block, therefore due to symmetry, the doublet is only moved towards the west block. The system lifetime criterion is defined in section System lifetime and NPV.

Appendix B. Supplementary data

Supplementary material related to this article can be found, in the online version, at doi:https://doi.org/10.1016/j.geothermics.2020.101806.

References

Altmann, J.B., Müller, B.I.R., Müller, T.M., Heidbach, O., Tingay, M.R.P., Weißhardt, A., 2014. Pore pressure stress coupling in 3D and consequences for reservoir stress states and fault reactivation. Geothermics. https://doi.org/10.1016/j.geothermics.2014.01.004.

Babaei, M., Nick, H.M., 2019. Performance of low-enthalpy geothermal systems: interplay of spatially correlated heterogeneity and well-doublet spacings. Appl. Energy 253, 113569. https://doi.org/10.1016/j.apenergy.2019.113569.

Barbier, E., 2002. Geothermal energy technology and current status: an overview. Renew. Sustain. Energy Rev. 6, 3–65. https://doi.org/10.1016/S1364-0321(02)00002-3.

Blöcher, M.G., Zimmermann, G., Moeck, I., Brandt, W., Hassanzadegan, A., Magri, F., 2010. 3D numerical modeling of hydrothermal processes during the lifetime of a deep geothermal reservoir. Geofluids 10, 406–421. https://doi.org/10.1111/j.1468-8123.2010.00284.x.

Bonté, D., Wees, J.D.Van, Verweij, J.M., 2012. Subsurface temperature of the onshore Netherlands: new temperature dataset and modelling. Netherlands J. Geosci. en Mijnb. 91, 491–515.

Chandrasiri Ekneligoda, T., Min, K.-B., 2014. Determination of optimum parameters of doublet system in a horizontally fractured geothermal reservoir. Renew. Energy 65, 152–160. https://doi.org/10.1016/j.renene.2013.08.003.

Crooijmans, R.A., Willems, C.J.L., Nick, H.M., Bruhn, D.F., 2016. The influence of facies heterogeneity on the doublet performance in low-enthalpy geothermal sedimentary reservoirs. Geothermics 64, 209–219. https://doi.org/10.1016/j.geothermics.2016.06.004.

Daniilidis, A., Herber, R., 2016. Salt Intrusions Providing a New Geothermal Exploration Target for Higher Energy Recovery at Shallower Depths. https://doi.org/10.1016/j.energy.2016.10.094.

Daniilidis, A., Doddema, L., Herber, R., 2016a. Risk assessment of the Groningen geothermal potential: from seismic to reservoir uncertainty using a discrete parameter analysis. Geothermics 64, 271–288. https://doi.org/10.1016/j.geothermics.2016.06.014.

Daniilidis, A., Doddema, L., Herber, R., 2016b. Risk assessment of the Groningen geothermal potential: from seismic to reservoir uncertainty using a discrete parameter analysis. Geothermics 64, 271–288. https://doi.org/10.1016/j.geothermics.2016.06.014.

Daniilidis, A., Alpsoy, B., Herber, R., 2017. Impact of technical and economic uncertainties on the economic performance of a deep geothermal heat system. Renew. Energy 114, 805–816. https://doi.org/10.1016/j.renene.2017.07.090.

Fox, D.B., Koch, D.L., Tester, J.W., 2015. The effect of spatial aperture variations on the thermal performance of discretely fractured geothermal reservoirs. Geotherm. Energy. https://doi.org/10.1186/s40517-015-0039-z.

Garg, S.K., Combs, J., 2015. A reformulation of USGS volumetric “heat in place” resource

estimation method. Geothermics 55, 150–158. https://doi.org/10.1016/J.GEOTHERMICS.2015.02.004.
Jalali, M., Embry, J.-M., Sanfilippo, F., Santarelli, F.J., Dusseault, M.B., 2016. Cross-flow analysis of injection wells in a multilayered reservoir. Petroleum 2, 273–281. https://doi.org/10.1016/J.PETLM.2016.05.005.
Jeanne, P., Rutqvist, J., Dobson, P.F., 2017. Influence of injection-induced cooling on deviatoric stress and shear reactivation of preexisting fractures in enhanced Geothermal Systems. Geothermics 70, 367–375. https://doi.org/10.1016/j.geothermics.2017.08.003.
Kim, S., Hosseini, S.A., 2015. Hydro-thermo-mechanical analysis during injection of cold fluid into a geologic formation. Int. J. Rock Mech. Min. Sci. 77, 220–236. https://doi.org/10.1016/j.ijrmms.2015.04.010.
Knoblauch, T.A.K., Trutnevyte, E., 2018. Siting enhanced geothermal systems (EGS): heat benefits versus induced seismicity risks from an investor and societal perspective. Energy 164, 1311–1325. https://doi.org/10.1016/j.energy.2018.04.129.
Lepillier, B., Daniilidis, A., Doonechaly Gholizadeh, N., Bruna, P.-O., Kummerow, J., Bruhn, D., 2019. A fracture flow permeability and stress dependency simulation applied to multi-reservoirs, multi-production scenarios analysis. Geotherm. Energy 7, 24. https://doi.org/10.1186/s40517-019-0141-8.
Liang, X., Xu, T., Feng, B., Jiang, Z., 2018. Optimization of heat extraction strategies in fault-controlled hydro-geothermal reservoirs. Energy 164, 853–870. https://doi.org/10.1016/J.ENERGY.2018.09.043.
Limberger, J., Boxem, T., Pluymaekers, M., Bruhn, D., Manzella, A., Calcagno, P., Beekman, F., Cloetingh, S., van Wees, J.-D., 2018. Geothermal energy in deep aquifers: a global assessment of the resource base for direct heat utilization. Renew. Sustain. Energy Rev. 82 (Part 1), 961–975. https://doi.org/10.1016/j.rser.2017.09.084.
Liu, G., Pu, H., Zhao, Z., Liu, Y., 2019. Coupled thermo-hydro-mechanical modeling on well pairs in heterogeneous porous geothermal reservoirs. Energy. https://doi.org/10.1016/j.energy.2019.01.022.
Madhur, G.B., Anderson, J.B., 2012. Sensitivity Analysis of Low-Temperature Geothermal Reservoirs: Effect of Reservoir Parameters on the Direct Use of Geothermal Energy. GRC Trans.
Moeck, I.S., 2014. Catalog of geothermal play types based on geologic controls. Renew. Sustain. Energy Rev. 37, 867–882. https://doi.org/10.1016/j.rser.2014.05.032.
Mottaghy, D., Pechnig, R., Vogt, C., 2011. The geothermal project Den Haag: 3D numerical models for temperature prediction and reservoir simulation. Geothermics 40, 199–210. https://doi.org/10.1016/j.geothermics.2011.07.001.
Saeid, S., Barends, F.B.J., 2009. An extension of Lauwerier's solution for heat flow in saturated porous media. Proc. COMSOL Conf. Milan, Oct. 2009 0.
Saeid, S., Al-Khoury, R., Nick, H.M., Barends, F., 2014. Experimental-numerical study of heat flow in deep low-enthalpy geothermal conditions. Renew. Energy 62, 716–730. https://doi.org/10.1016/j.renene.2013.08.037.
Saeid, S., Al-Khoury, R., Nick, H.M., Hicks, M.A., 2015. A prototype design model for deep low-enthalpy hydrothermal systems. Renew. Energy 77, 408–422. https://doi.org/10.1016/j.renene.2014.12.018.
Salimzadeh, S., Nick, H.M., 2019. A coupled model for reactive flow through deformable fractures in enhanced Geothermal Systems. Geothermics 81, 88–100. https://doi.org/10.1016/J.GEOTHERMICS.2019.04.010.
Salimzadeh, S., Nick, H.M., Zimmerman, R.W., 2018. Thermoporoelastic effects during heat extraction from low-permeability reservoirs. Energy. https://doi.org/10.1016/j.energy.2017.10.059.
Salimzadeh, S., Grandahl, M., Medetbekova, M., Nick, H.M., 2019. A novel radial jet drilling stimulation technique for enhancing heat recovery from fractured geothermal reservoirs. Renew. Energy. https://doi.org/10.1016/j.renene.2019.02.073.
Slatlem Vik, H., Salimzadeh, S., Nick, H.M., 2018. Heat recovery from multiple-fracture enhanced geothermal systems: the effect of thermoelastic fracture interactions. Renew. Energy 121, 606–622. https://doi.org/10.1016/J.RENENE.2018.01.039.
TNO, 2018. ThermoGIS v2.0 - Economic Model [WWW Document]. ThermoGIS v2.0. URL https://www.thermogis.nl/en/economic-model (accessed 7.2.19). .
van Os, H.W.A., Herber, R., Scholtens, B., 2016. Subsurface activities and decision support systems: an analysis of the requirements for a social acceptance-motivated decision support system. Environ. Impact Assess. Rev. 60, 176–185. https://doi.org/10.1016/J.EIAR.2016.06.002.
Vogt, C., Iwanowski-Strahser, K., Marquart, G., Arnold, J., Mottaghy, D., Pechnig, R., Gnjezda, D., Clauser, C., 2013. Modeling contribution to risk assessment of thermal production power for geothermal reservoirs. Renew. Energy 53, 230–241. https://doi.org/10.1016/j.renene.2012.11.026.
Watanabe, N., Wang, W., McDermott, C.I., Taniguchi, T., Kolditz, O., 2010. Uncertainty analysis of thermo-hydro-mechanical coupled processes in heterogeneous porous media. Comput. Mech. https://doi.org/10.1007/s00466-009-0445-9.
Willems, C.J.L., Nick, H.M., 2019. Towards optimisation of geothermal heat recovery: an example from the West Netherlands Basin. Appl. Energy 247, 582–593. https://doi.org/10.1016/j.apenergy.2019.04.083.
Willems, C.J.L., Nick, H.M., Goense, T., Bruhn, D.F., 2017a. The impact of reduction of doublet well spacing on the Net Present Value and the life time of fluvial Hot Sedimentary Aquifer doublets. Geothermics 68, 54–66. https://doi.org/10.1016/j.geothermics.2017.02.008.
Willems, Cees J.L., Nick, H.M., Weltje, G.J., Bruhn, D.F., 2017b. An evaluation of interferences in heat production from low enthalpy geothermal doublets systems. Energy 135, 500–512. https://doi.org/10.1016/J.ENERGY.2017.06.129.